Supporting Information

Breaking the kinetic limitation of formaldehyde oxidation by Ag-doping modulation of *H adsorption on Cu_2O

Qing Liao[a], Weijie Li[b], Yi Wei[a,*], Chao Han[a,*]

[a] School of Materials Science and Engineering, Central South University, Changsha 4100083, Hunan Province, P. R. China

[b] Powder Metallurgy Research Institute, Central South University, Changsha 410083, Hunan Province, P. R. China

* Corresponding author

E-mail: chaohan@csu.edu.cn

1. Experimental Procedures

1.1. Chemicals and reagents

Potassium hydroxide (KOH, 95%), Silver nitrate ($AgNO_3$), copper sulfate, hydrogen peroxide (H_2O_2), heavy water (D_2O), dimethylformamide (DMSO, ≥99.9%, HPLC), anhydrous ethanol (CH_3CH_2OH, AR), methanol (CH_3OH), formaldehyde (HCHO, 37% wt in H_2O, 10%-15% CH_3OH Stabilizer), formic acid (HCOOH), potassium hydroxide (KOH, 99.99%), hydrochloric acid (HCl，36.0%-38.0%, AR). The entire experimental process utilized ultrapure water (18.25 MΩ cm^{-1}) from a water purification system.

1.2. Materials and Methods

1.2.1. Synthesis of Ag@Cu_2O/CF

First, a piece of foam copper (1 × 1 cm) was sequentially ultrasonicated in anhydrous ethanol, 1 M hydrochloric acid solution, and ultrapure water for 5 minutes each. Subsequently, predetermined amounts of potassium hydroxide, hydrogen peroxide, and silver nitrate were introduced into a beaker and magnetically stirred until a homogeneous mixture was obtained (the beaker was shielded from light with aluminum foil during this process). The treated foam copper was then immersed in the resulting mixture for 2 hours. After reaction, the sample was washed three times each with ultrapure water and anhydrous ethanol, and finally dried in a vacuum oven at 60 °C for 6 hours to yield Ag@Cu_2O/CF. Samples prepared with the addition of 1, 3, and 5 mmol of silver nitrate were labeled as Ag_1@Cu_2O/CF, Ag@Cu_2O/CF, and Ag_3@Cu_2O/CF, respectively.

1.2.2. Synthesis of Cu_2O/CF

The synthesis of Cu_2O/CF is similar to that of Ag@Cu_2O/CF, with the key difference being that silver nitrate is not added when preparing the mixed solution. Consequently, the resulting product is Cu_2O/CF.

1.2.3. Synthesis of Ag_2O/CF

The synthesis of Ag_2O/CF involves immersing pretreated sponge copper in a silver

nitrate solution to obtain the resulting product.

1.3. Physical characterizations

X-ray diffraction (XRD) analysis was performed using a Rigaku SmartLab diffractometer with Cu-Kα radiation (λ = 0.154 nm), with data collected over a 2θ range of 10° to 100°. Morphological examination utilized a Nova Nano SEM 450 field-emission scanning electron microscope operated at 15 kV, while elemental distribution mapping employed energy-dispersive X-ray spectroscopy (EDS, JEOL JEM-1400-plus). High-resolution transmission electron microscopy (HRTEM), aberration-corrected high-angle annular dark-field scanning TEM (AC-HAADF-STEM) images, and energy-dispersive X-ray spectroscopy (EDS) maps were acquired using a JEOL JEM-F200 transmission electron microscope. Inductively coupled plasma-optical emission spectrometry (ICP-OES) was conducted using a PerkinElmer Avio 500. The test involves scraping the surface of sample by a steel knife, then the obtained sample was dissolved nitric acid, followed by testing the Ag concentration by ICP-OES measurement. X-ray photoelectron spectroscopy (XPS) analysis was conducted using a Thermo Fisher Scientific K-Alpha photoelectron spectrometer. Ultraviolet photoelectron spectroscopy (UPS) was conducted using a Thermo Fisher Scientific Escalab 250Xi photoelectron spectrometer. Raman spectroscopy was performed using a Thermo Scientific drx3 Raman microscope. Fourier transform infrared (FT-IR) spectroscopy was performed using a PerkinElmer Spectrum 3 spectrometer, with spectra collected in the mid-infrared region (400-4000 cm^{-1}). Liquid products were analyzed using a proton nuclear magnetic resonance (^1H NMR) spectrometer (Bruker Advance Neo 600 MHz). Gaseous products were analyzed online using a gas chromatograph (Fuli GC9790plus) equipped with a thermal conductivity detector (TCD).

1.4. Electrochemical measurements

The CS2350M dual-potentiostat (Kostar, China) and the GSR C007-1 replaceable membrane H-type cell were employed. Foam copper samples served as working

electrodes with an actual immersion area of 0.5 × 0.5 cm² in the electrolyte. An Ag/AgCl electrode (in saturated KCl solution) was used as the reference electrode, placed in the same cell chamber as the working electrode. The counter electrode in the other cell chamber was a ruthenium-yttrium-titanium electrode (1 × 1 cm^2).

Measured potentials were calculated using the reversible hydrogen electron potential from the Nernst equation:

$$E_{RHE} = E_{Ag/AgCl} + 0.0592 \times pH + 0.197$$

All reported potentials were without IR drop compensation. For the electrocatalytic formaldehyde oxidation reaction, the cathode solution was 35 mL 1 M KOH, and the anode solution was 35 mL 1 M KOH + 0.2 M HCHO. Throughout the measurements, the formaldehyde-containing anolyte was stirred at high speed. Linear sweep voltammetry was performed at a scan rate of 5 mV/s. The I-t test was conducted continuously for 3 h at 0.35 V vs. RHE. Electrochemical impedance spectroscopy was performed at a working voltage of 0 V, amplitude of 5 mV, and frequency range of 10^6 to 10^{-1} Hz. Electrochemical surface area (ECSA) was calculated from the double-layer capacitance (C_{dl}) through a CV method. Specifically, the CV measurements wereconducted at different scan rates in a potential range of 0.1-0.2 V vs. RHE electrode(no Faradic responses). Then, the values of C_{dl} were calculated by plotting capacitivecurrent density Δj (janode - jcathode, acquired from the corresponding CV curves in Fig. S11) at 0.15 V vs. RHE electrode versus scan rate, and the linear slope value is twice that of the C_{dl}. Therefore, the ECSA values were calculated based on theS5following equation: ECSA = (C_{dl}·S)/Cs, where S is the geometric area of the workingelectrode and Cs is the specific capacitance of a smooth surface (generally assumed tobe 0.04 mF cm^{-2}). In the bipolar hydrogen evolution cell, Ag_2@Cu_2O/CF and Pt/C (1 × 1 cm^2) were employed as the anode and cathode, respectively, with a mass loading of 1.0 mg cm^{-2} for both.

1.5. In-situ ATR-FTIR, online DEMS measurements

All in-situ spectroscopic measurements were conducted using a three-electrode electrochemical cell containing electrolyte of 1 M KOH and 0.2 M HCHO, with

Ag@Cu_2O/CF, Pt wire and Ag/AgCl electrode serving as the working, counter and reference electrodes, respectively.

At-the-spot attenuated total reflection Fourier transform infrared (ATR-FTIR) measurements were performed using a PerkinElmer Spectrum 3 instrument. The ATR technique employed a single-reflection silicon crystal coated with an Au film in the internal reflection mode. Ag@Cu_2O/CF was compressed into thin sheets, cut to the size of rubber rings, and placed between the rubber ring and the Au film to serve as the working electrode. Before measurements, the background spectrum was obtained at open-circuit potential, while other spectra were collected over the potential range from open-circuit potential to 0.5 V vs. RHE. Reaction intermediates were monitored online using a QAS-100 differential electrochemical spectrometer (Shanghai Linglu Instruments). Mass signals were continuously acquired during CV scans from -0.2 V vs. RHE to 0.4 V vs. RHE at a scan rate of 10 mV/s. To ensure accuracy, six cycles were tested under identical conditions.

1.6. ^{1}H NMR determination of formate

Using dimethyl sulfoxide (DMSO) solution as an internal standard, formate was identified and quantified via nuclear magnetic resonance (NMR) hydrogen spectroscopy. For NMR hydrogen spectroscopy analysis, add 250 μL of 1 M hydrochloric acid solution to 250 μL of electrolyte solution, 100 μL of heavy water, and 200 μL of 200 ppm DMSO solution to form an 800 μL mixture. After thorough shaking, 500 μL was transferred to a ^{1}H NMR tube for testing. A series of solutions containing target formate derivatives at known concentrations was prepared to establish the corresponding standard calibration curve.

1.7. Calculations of Faradaic efficiency (FE), yield, yield rate, conversion rate, energy efficiency and collection efficiency

The H_2 gas production was collected by the downward drainage method. The actually produced H_2 amount was calculated as follows:

$$n[mole]_{actually\ produced} = V_{H2} \div V_m$$

The theoretically produced H_2 amount was calculated as follows:

$$n[mole]_{theoretically\ produced} = Q \div (n \times F)$$

The FE of formate was calculated as follows:

$$FE_{acid} = \left(n_{mole\ acid} \times n \times F\right) \div Q \times 100\%$$

The power consumed per m^3 H_2 generated (W, kWh per m^3 H_2) was calculated as follows:

$$W = (n \times F \times U \times 1000) \div (3600 \times V_m)$$

Where F is the Faraday constant (96,485 C/mol), V is the volume of the electrolyte, Q is the total charge passing the electrode, V_{H2} is the volume of H_2 gas collected, n[mole] is the mole number of the substrate, n is the number of electrons transferred for each product molecule, n is the number of electrons transferred per product molecule, U is the applied voltage, and Vm is the molar volume of a gas at room temperature and pressure (24.5 mol/L), n=1 in bipolar hydrogen production system and n=2 in traditional hydroelectrolysis system.

1.8. Computing details

All the DFT calculations were conducted based on the Vienna Ab initio Simulation Package (VASP)[1, 2]. The exchange-correlation potential was described by the Perdew−Burke−Ernzerhof (PBE) generalized gradient approach (GGA)[3]. The electron-ion interactions were accounted for by the projector augmented wave (PAW)[4]. All DFT calculations were performed with a cut-off energy of 500 eV, and the Brillouin zone was sampled using a 3 × 3 × 1 k-point grid. The energy and force convergence criteria of the self-consistent iteration were set to 10^{-5} eV and 0.02 eV $Å^{-1}$, respectively. The DFT-D3 method was used to describe van der Waals (vdW) interactions[5].The Gibbs free energy changes (ΔG) of the reaction are calculated using the following formula:

$$\Delta G = \Delta E + \Delta ZPE - T\Delta S + \Delta G_u + \Delta G_{pH}$$

Where ΔE is the difference of electron energies calculated by DFT; ΔZPE and ΔS are the changes of zero-point energy and entropy, respectively, which are obtained from vibrational frequencies. T is the temperature (298.15 K). $\Delta G_U = -eU$, where U is the

applied electrode potential. $\Delta G_{pH} = k_B T \times ln10 \times pH$ where k_B is the Boltzmann constant.

2. Results and discussion

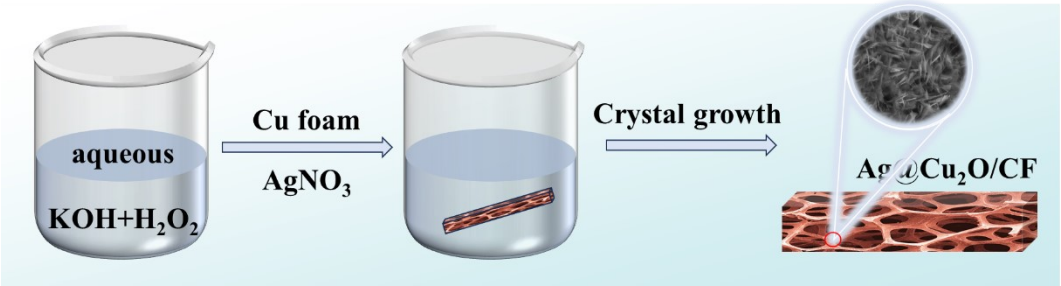

Fig. S1 Flowchart for the Synthesis of Ag@Cu_2O samples with different Ag contents.

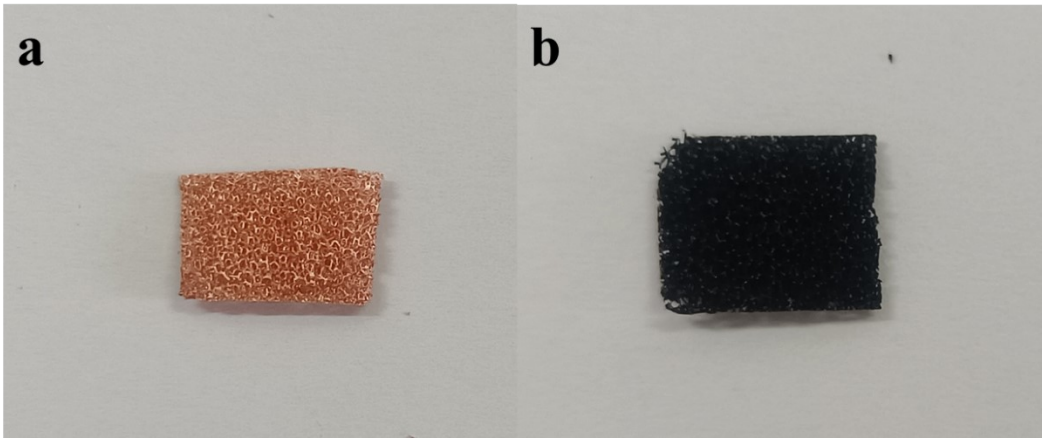

Fig. S2 Photographs of (a) CF and (b) Ag@Cu_2O loaded CF

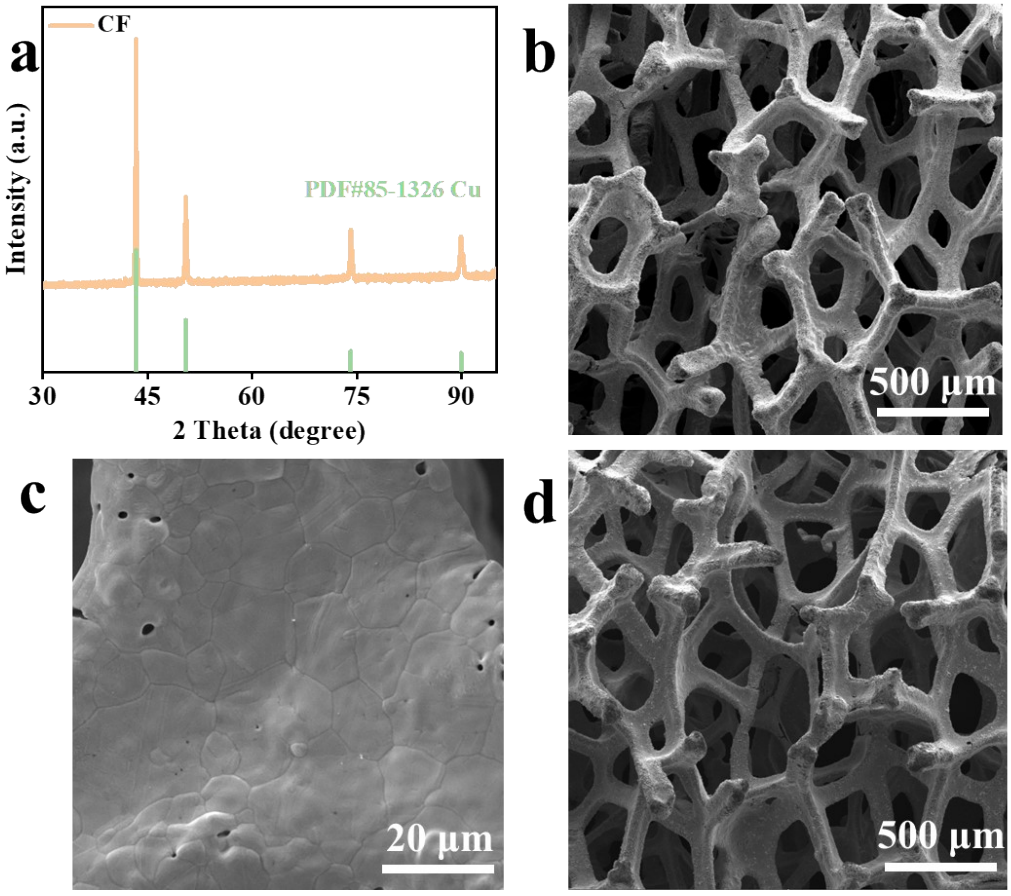

Fig. S3 (a) XRD of CF. (b) SEM of CF after pretreatment. (c) SEM of CF after pretreatment. (d) SEM Ag@Cu_2O/CF. After pretreatment, the foam copper retains its porous skeletal structure with a smooth surface. Combined with XRD results, it is evident that surface oxides and oils have been thoroughly removed.

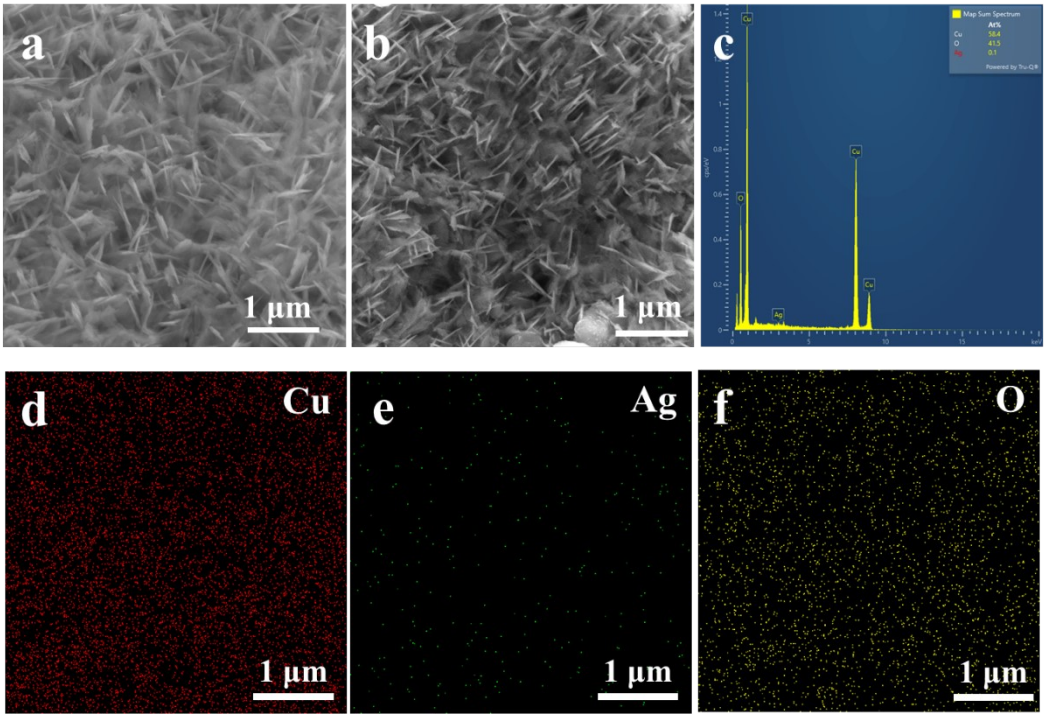

Fig. S4 SEM and EDS of Ag@Cu_2O/CF. (a) SEM of Ag@Cu_2O/CF. (b) SEM of Ag@Cu_2O/CF. (c) EDS of Ag@Cu_2O/CF. (d) EDS mapping of Cu. (e) EDS mapping of Ag. (f) EDS mapping of O.

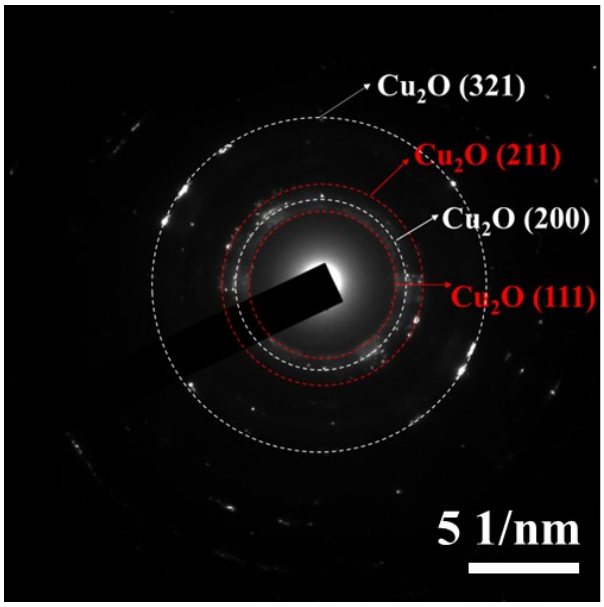

Fig. S5 Selective area electron diffraction pattern of Ag@Cu_2O/CF.

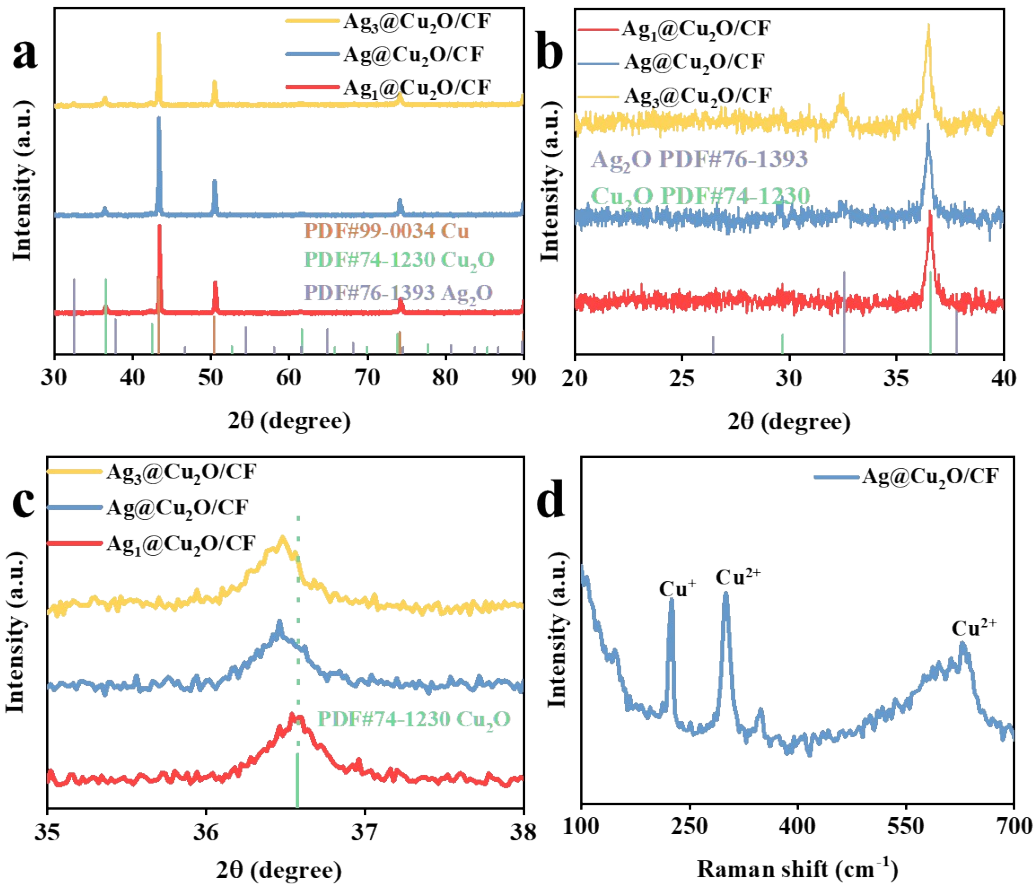

Fig. S6 (a) XRD patterns of $Ag_1@Cu_2O/CF$, $Ag@Cu_2O/CF$, $Ag_3@Cu_2O/CF$. (b) XRD pattern amplified in the 2Θ range of 20-40. (c) XRD pattern amplified in the 2Θ range of 35-38. (d) Raman spectrum of $Ag@Cu_2O/CF$. The signal at 224 cm^{-1} corresponds to Cu^+, while those at 300 cm^{-1} and 600 cm^{-1} correspond to Cu^{2+}. This indicates partial oxidation on the sample surface.

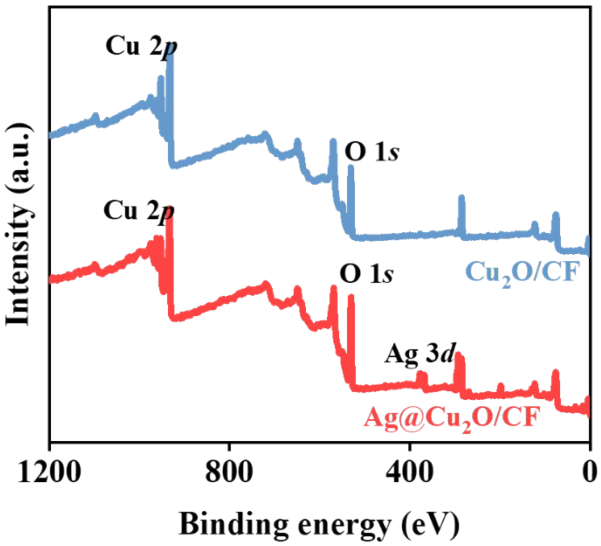

Fig. S7 Survey XPS spectra of Cu_2O/CF and Ag@Cu_2O/CF. The XPS survey spectra confirmed the presence of Ag, Cu and O elements exclusively in Ag@Cu_2O/CF.

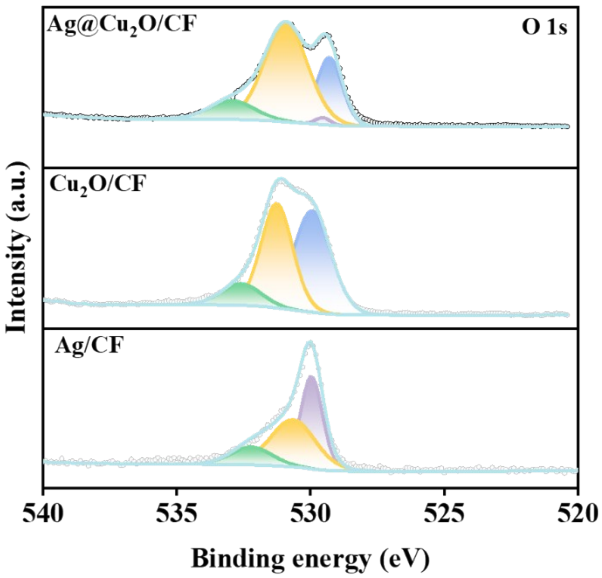

Fig. S8 High-resolution O 1s XPS spectra of Ag@Cu_2O/CF.

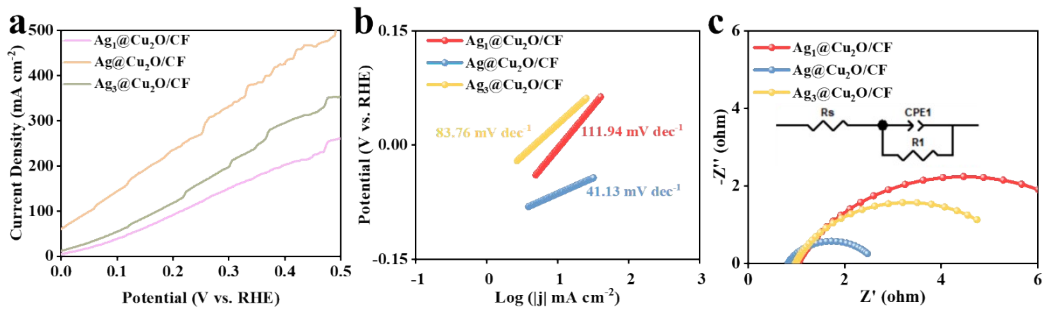

Fig. S9 (a) LSVs of Ag_1@Cu_2O/CF, Ag@Cu_2O/CF, Ag_3@Cu_2O/CF. (b) Tafel curves

of $Ag_1@Cu_2O/CF$, $Ag@Cu_2O/CF$, $Ag_3@Cu_2O/CF$. (c) EIS curves of $Ag_1@Cu_2O/CF$, $Ag@Cu_2O/CF$, $Ag_3@Cu_2O/CF$

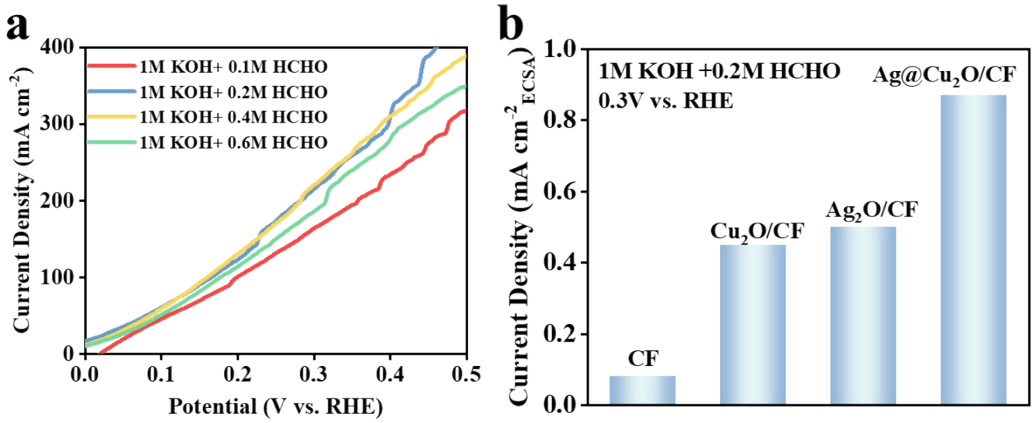

Fig. S10 LSV was performed on the $Ag@Cu_2O/CF$ electrode at a scan rate of 5 mV/s in 1 M KOH electrolytes containing varying concentrations of formaldehyde (HCHO). (b) Normalized current density by ECSA at 0.3 V vs. RHE.

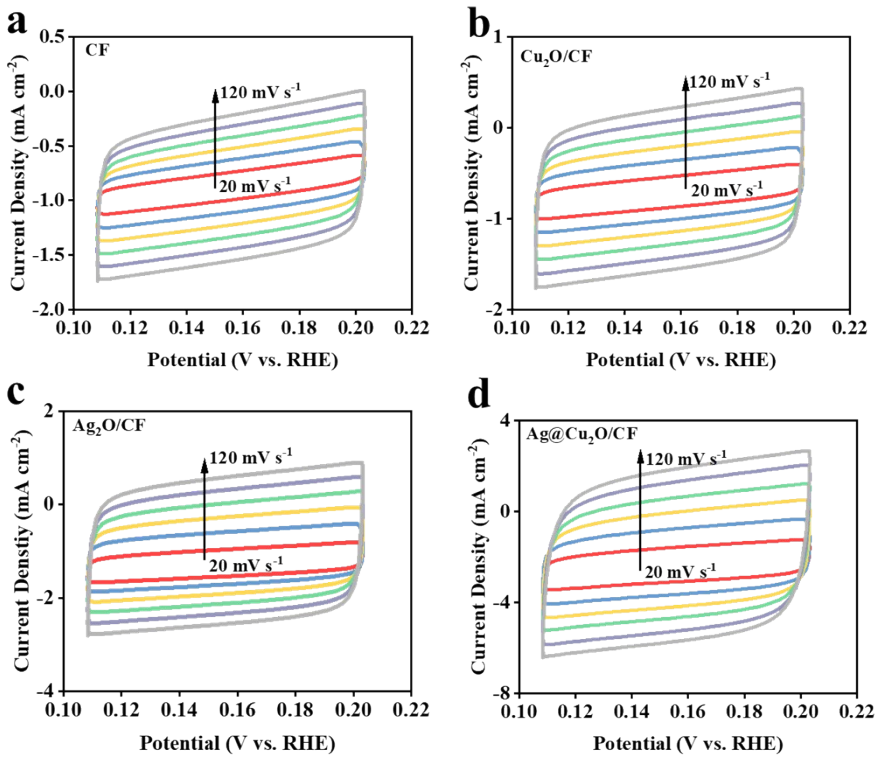

Fig. S11 Cyclic voltammetry curve in 1.0 M KOH electrolyte. (a) CF; (b) Cu_2O/CF; (c) Ag_2O/CF; (d) $Ag@Cu_2O/CF$.

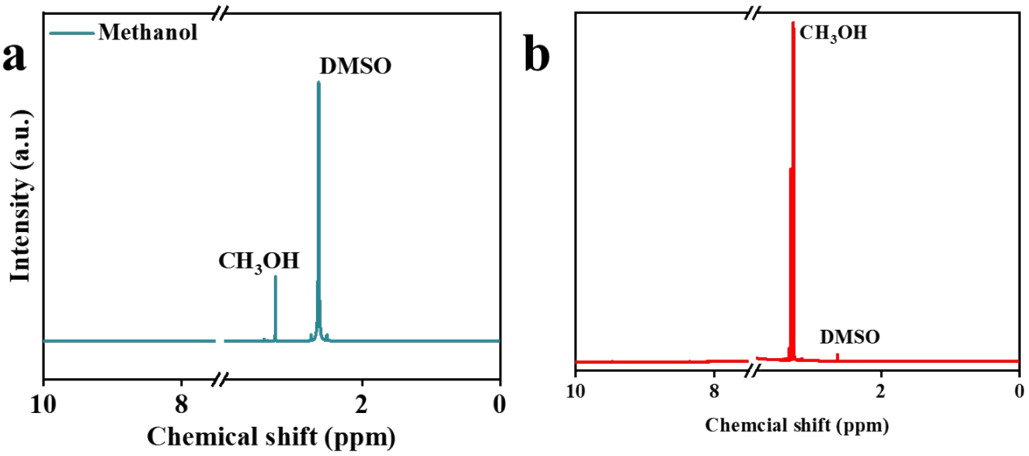

Fig. S12 (a) NMR Spectrum of Methanol Reference Material. (b) NMR spectrum of 1.0 M KOH + 0.2 M HCHO electrolyte after standing for two days.

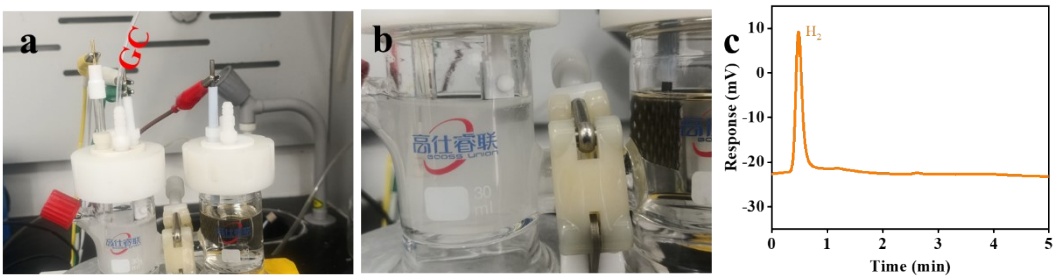

Fig. S13 (a) Schematic of the H-type reactor. (b) Bubble formation on the working electrode surface during the FOR reaction; (c) Gas phase product detection chart for FOR (GC9790 plus)

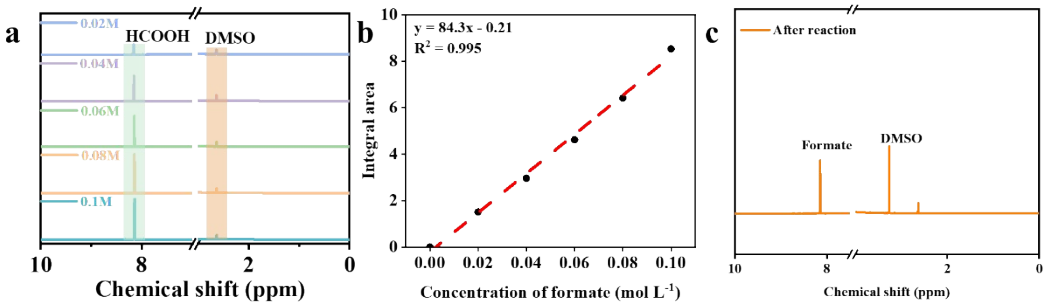

Fig. S14 (a) ^{1}H-NMR curves of formate at different concentrations. (b) Standard curve for the formate quantification. (c) ^{1}H-NMR curves of the format after reaction.

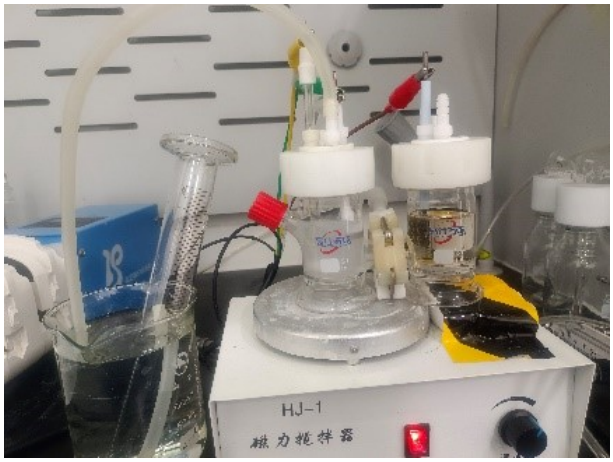

Fig. S15 Hydrogen collection by drainage method diagram.

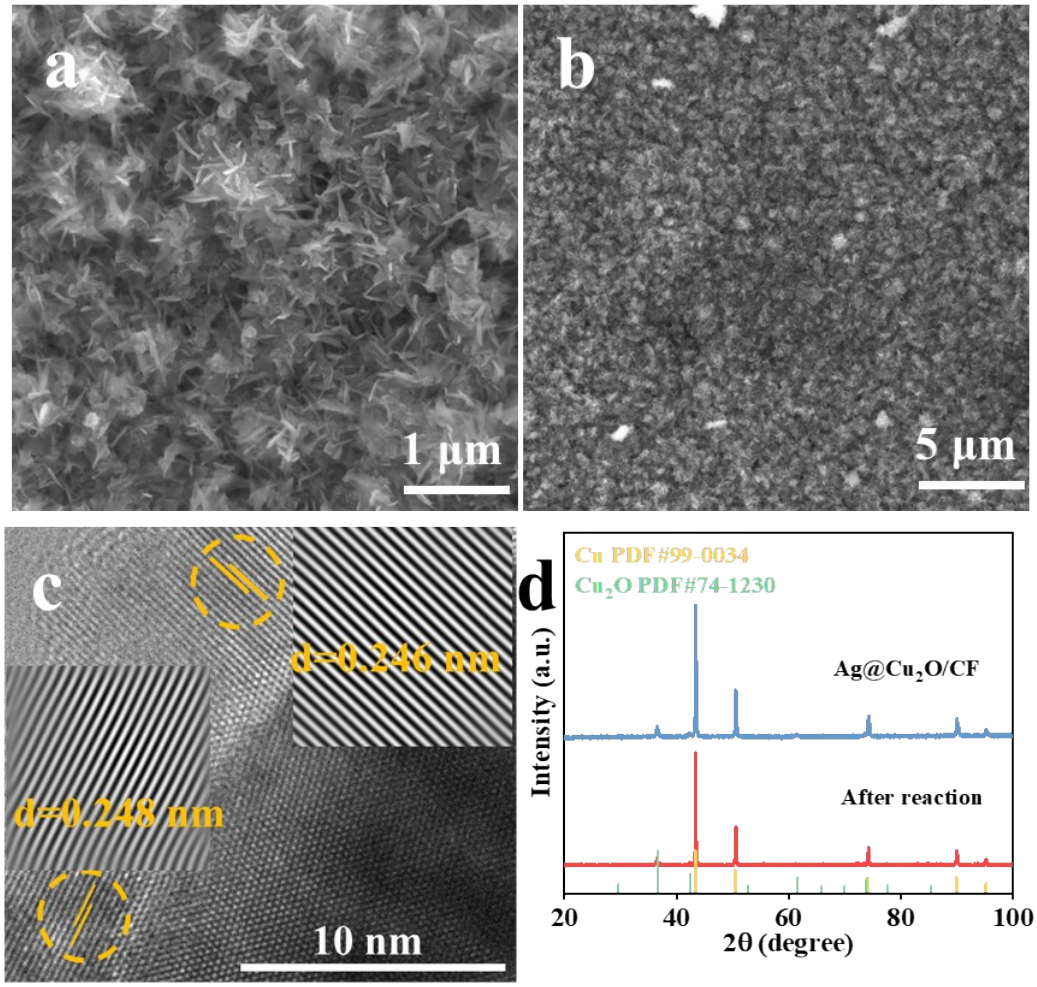

Fig. S16 (a) and (b) show SEM images of Ag@Cu_2O/CF after completing the stability test. (c) TEM of Ag@Cu_2O/CF after stability testing. (d) Comparison of XRD Patterns Before and After

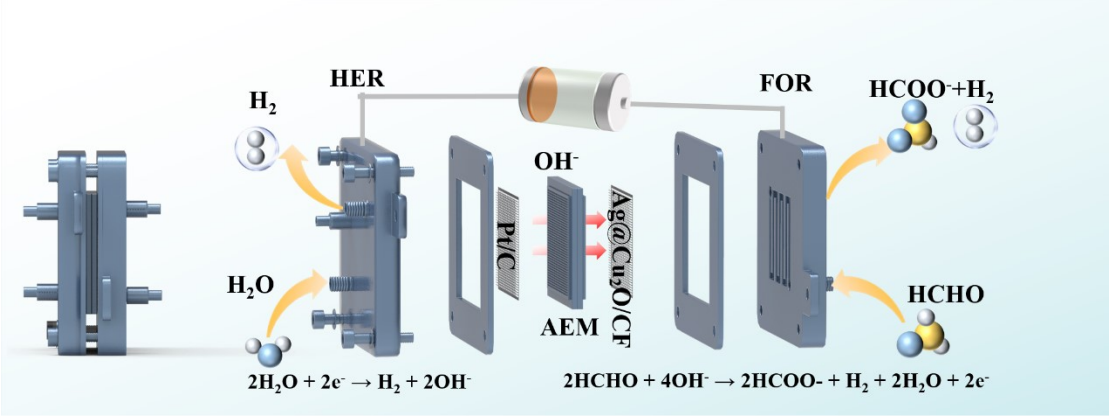

Fig.S17 Schematic diagram of bipolar hydrogen production.

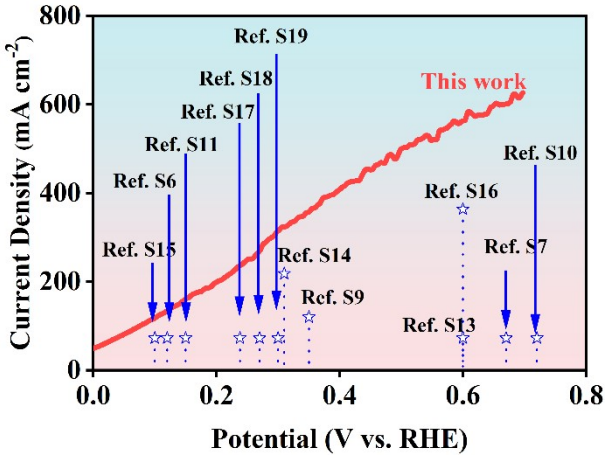

Fig. S18 Comparison of hydrogen production potential on different substrate anodes, all the mentioned references are listed in the supporting information.

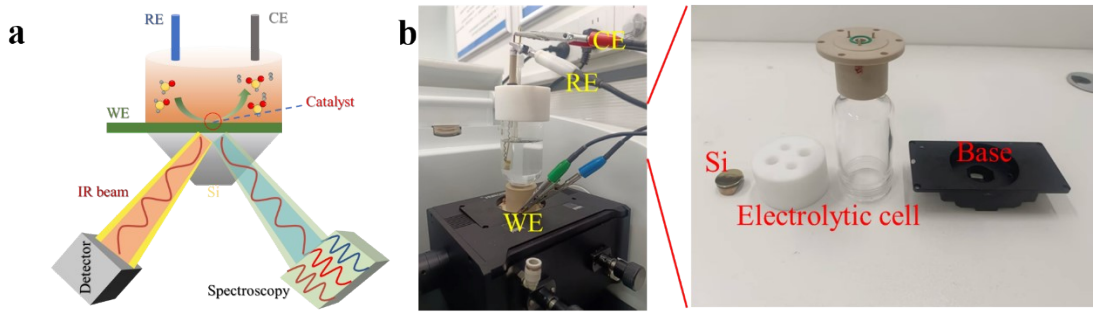

Fig. S19 Schematic diagram of the in-situ infrared spectra.

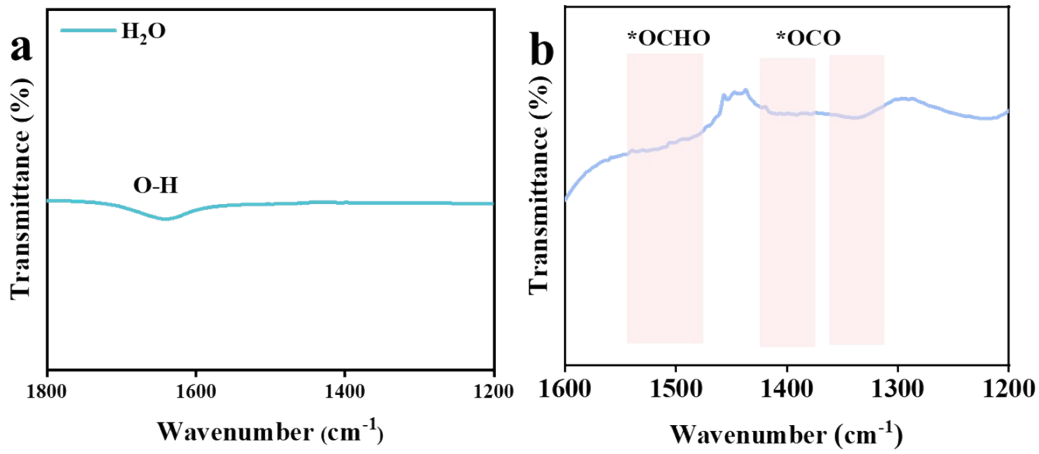

Fig. S20 (a) ATR-SEIRAS measurements in pure KOH solution. (b) ATR-SEIRAS in KOH containing 0.5 M HCOOK.

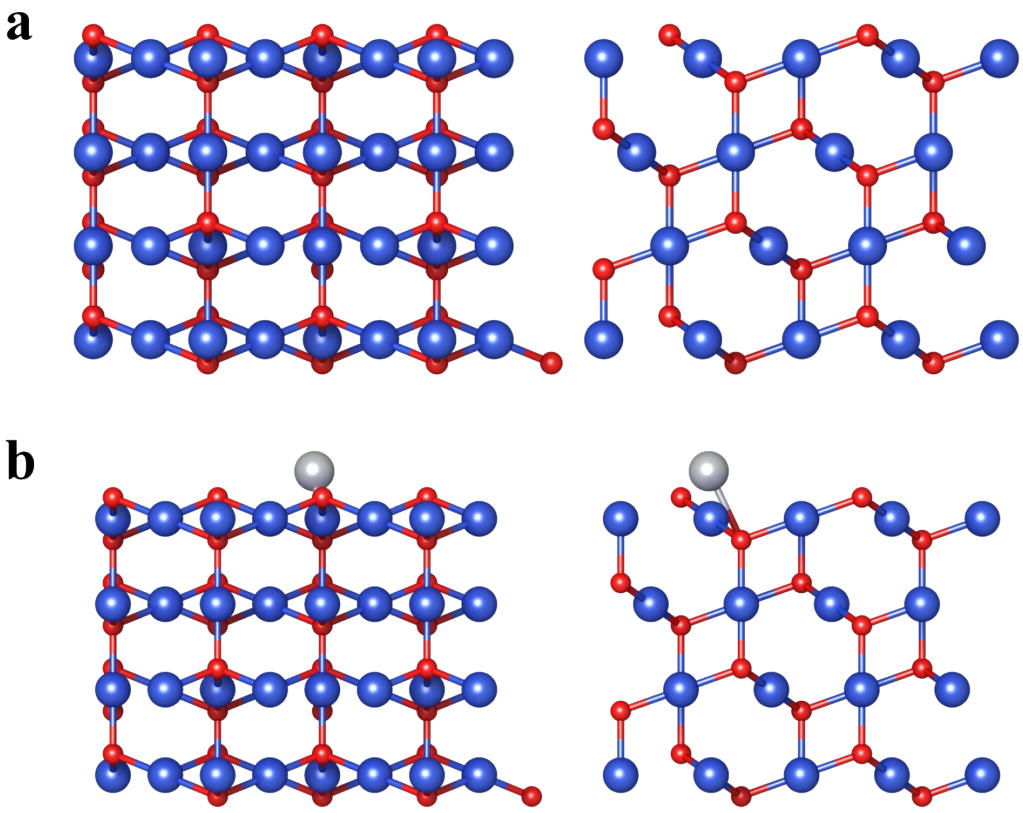

Fig. S21 Models of the (111) surfaces of (a) Cu_2O, (b) Ag@Cu_2O/CF.

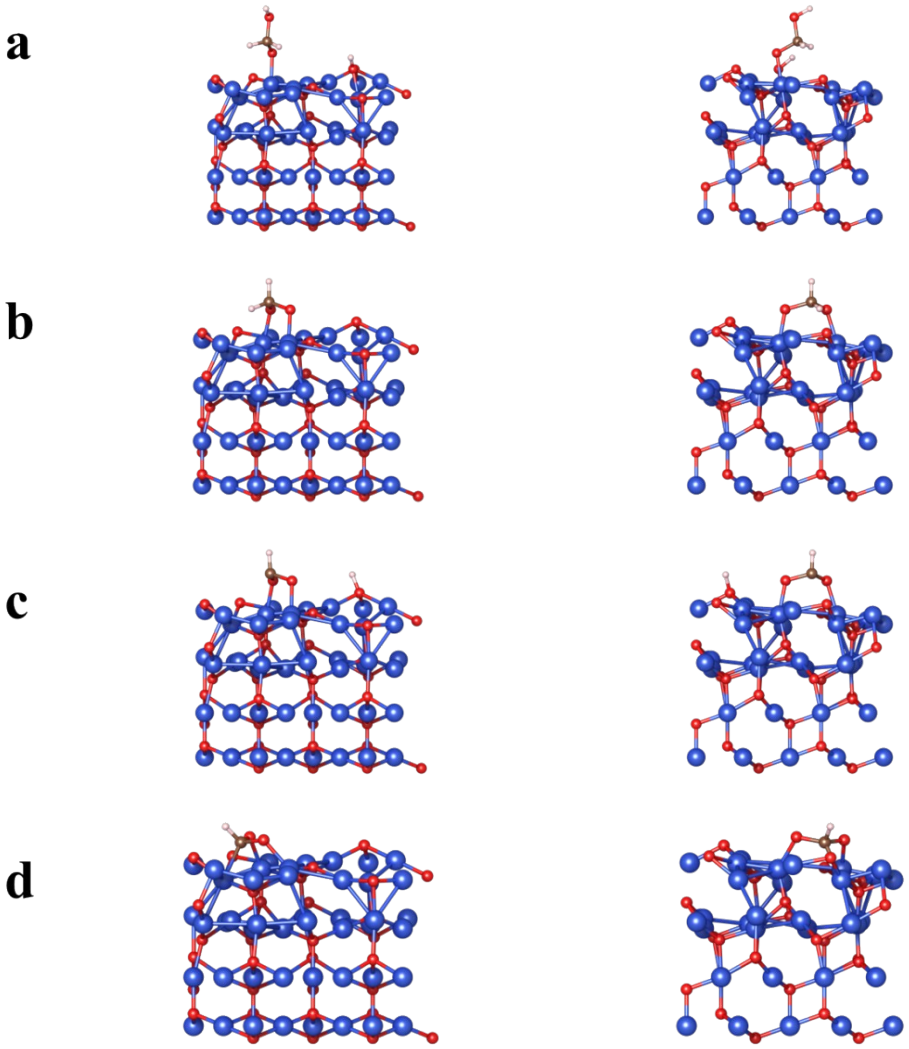

Fig. S22 The geometry of $^{*}O(OH)CH_2$ + $^{*}OH$, $^{*}OCH_2O^{*}$, $^{*}OOCH$+ $^{*}H$ and $^{*}OOCH$ adsorbed on the Cu_2O catalyst.

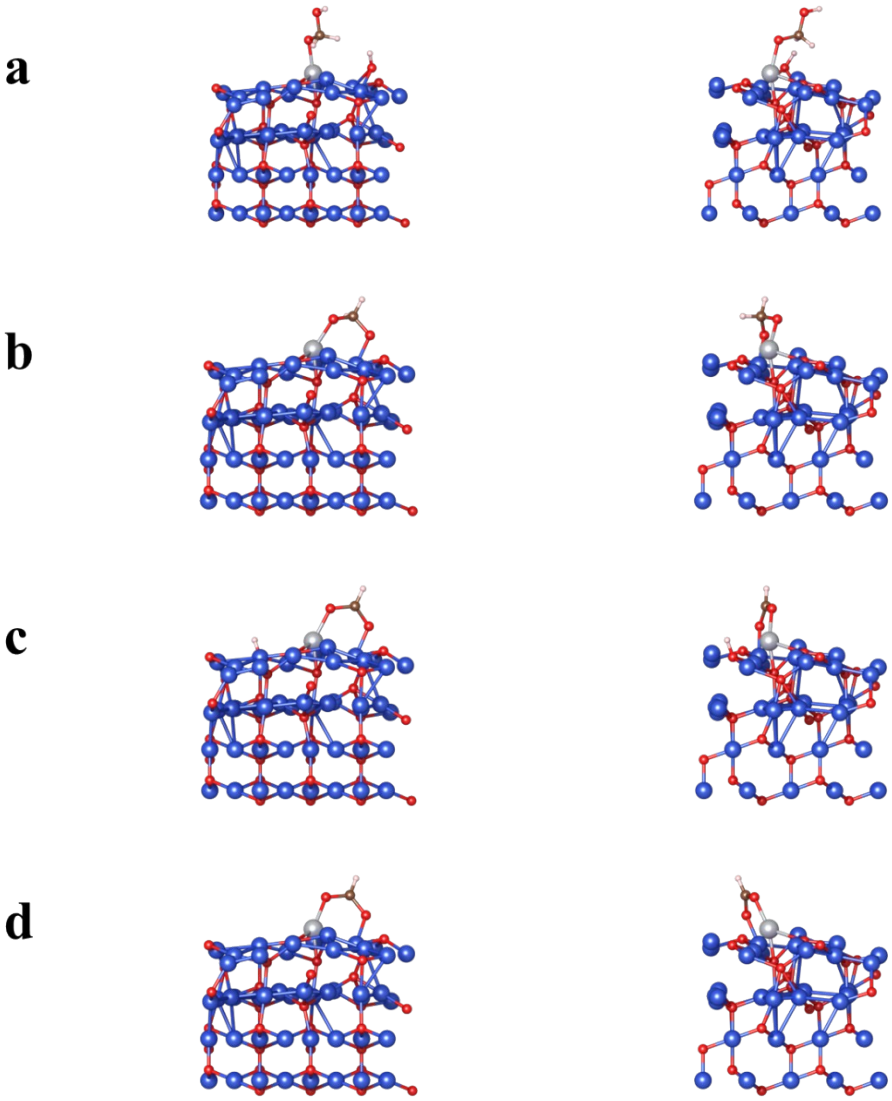

Fig. S23 The geometry of $^{*}O(OH)CH_2$ + $^{*}OH$, $^{*}OCH_2O^{*}$, $^{*}OOCH$+ $^{*}H$ and $^{*}OOCH$ adsorbed on the $Ag@Cu_2O$ catalyst.

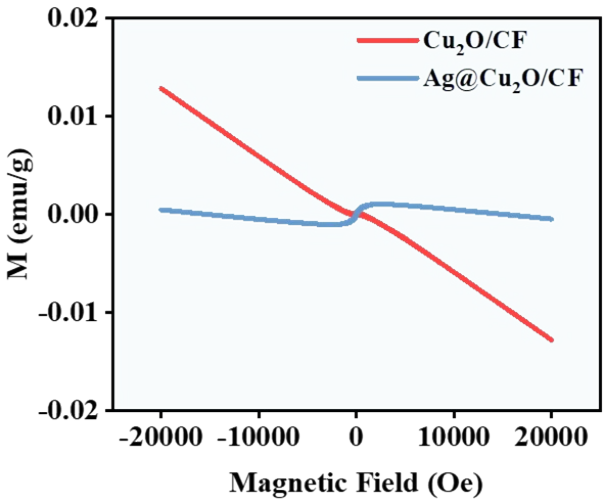

Fig. S24 Hysteresis loop data of Ag@Cu_2O/CF and Cu_2O/CF. Cu_2O/CF shows anti-ferromagnetic property, and Ag@Cu_2O/CF shows paramagnetic property.

3. Supplementary Tables

Table S1. ICP testing data results

Element	Weight (g)	Volume (mL)	Dilution factor	Sample concentration	Unit	Percentage by mass (%)
Ag	0.0365	50	1	1288.4096	mg/Kg	0.1288

Table S2. Comparison of the actual and theoretical amount of H_2 produced during electrocatalytic FOR on Ag@Cu_2O/CF

Charge(C)	$n(mmol)_{theoretically\ produced}$	$n\ (mmol)_{actually\ produced}$
0	0	0
50	0.26	0.26
100	0.52	0.49
150	0.78	0.77
200	1.04	1.03

Table S3. Comparison of the electrocatalytic FOR performance between $Ag@Cu_2O/CF$ and previously reported catalysts.

Catalyst	Electrolyte	Potential (V vs. RHE)	Current density (A cm^{-2})	Ref.
$Ag@Cu_2O/CF$	1 M KOH + 0.2 M HCHO	0.05	0.1	This work
Pt SA-Cu NWs	1 M KOH + 0.2 M HCHO	0.12	0.1	[6]
Pd	1 M KOH + 0.6 M HCHO	0.670	0.1	[7]
Pt_1Cu-CF	1 M KOH + 0.5 M HCHO	1.05	1	[8]
$Cu_xO@CF$	1 M KOH + 0.5 M HCHO	0.35	0.165	[9]
$Pd-Cu/Cu_2O/CF$	1 M KOH + 0.3 M HCHO	0.72	0.1	[10]
S-OH Cu	1 M KOH + 0.1 M HCHO	0.15	0.1	[11]
Cu@Ni（OH）$_2$/CF	1 M KOH + 0.25 M HCHO	0.36	0.5	[12]
Pu@Cu	0.5 M KOH + 0.1 M HCHO	0.6	0.1	[13]
$Ag_1@Cu_2O$ NWS	1 M KOH + 0.2 M HCHO	0.31	0.3	[14]
$RuCe-Cu_2O/CF$	1 M KOH + 0.2 M HCHO	0.1	0.1	[15]
CuFe@CF	1 M KOH + 0.2 M HCHO	0.6	0.5	[16]
Cu_2O	1 M KOH + 0.1 M HCHO	0.238	0.1	[17]
Cu_3Ag_7/CF	1 M KOH + 0.6 M HCHO	~0.27	0.1	[18]
Cu_2O	1 M KOH + 1.0 M HCHO	~0.3	0.1	[19]

4. References

1. G. Kresse and J. Hafner, *Phys. Rev. B*, 1993, **47**, 558-561.
2. G. Kresse and J. Hafner, *Phys. Rev. B*, 1994, **49**, 14251-14269.
3. J. P. Perdew, K. Burke and M. Ernzerhof, *Phys. Rev. Lett.*, 1996, **77**, 3865-3868.
4. G. Kresse and D. Joubert, *Phys. Rev. B*, 1999, **59**, 1758-1775.
5. S. Grimme, J. Antony, S. Ehrlich and H. Krieg, *J. Chem. Phys.*, 2010, **132**, 154104.
6. J. Qiu, X. Gao and J. Peng, *Chem. Eng. J.*, 2025, **513**, 162961.
7. G. Han, G. Li and Y. Sun, *Nat. Catal.*, 2023, **6**, 224-233.
8. J. Song, D. Xiao, J. He, C. Zhang, Q. Zhang, Z. Wang, Y. Liu, Z. Zheng, H. Cheng, Y. Wu, B. Huang and P. Wang, *Energy Environ. Sci.*, 2025, **18**, 6106-6116.
9. Y. Pan, Y. Li, C.-L. Dong, Y.-C. Huang, J. Wu, J. Shi, Y. Lu, M. Yang, S. Wang and Y. Zou, *Chem*, 2023, **9**, 963-977.
10. H. Yu, W. Liu, S. Jiang, L. Zhang, K. Deng, Z. Wang, Y. Xu, H. Wang and L. Wang, *Chem. Commun.*, 2025, **61**, 10554-10557.
11. D. Liu, Z. Yang, F. Si, X. Kang, H. You, H. Chen, Y. Weng, G. Fu, J. Zhang, X.-Z. Fu and J.-L. Luo, *Nano Res.*, 2025, **18**, 94907646.
12. S. Jiang, Y. Liu, R. Yang, L. Zhang, W. Liu, K. Deng, H. Yu, H. Wang and L. Wang, *Small*, 2025, **21**, 2410478.
13. C. Ye, Y. Yang, S. Chen, C. Liu, X.-Q. Sun, D. Liu, J. Zhang, J.-L. Luo and X.-Z. Fu, *Chem. Eng. J.*, 2025, **524**, 168224.
14. L. Zhang, Y. Cai, Y. Li, C. Sun, Y. Xiao, Y. Yang, D. Chen, D. Xiao, C.-F. Lee, Y. Wang, S. Feng, H.-T. Wang, Y.-C. Shao, T.-S. Chan, H. Ishii, N. Hiraoka, X. Wang, J. Luo and L. Han, *Energy Environ. Sci.*, 2025, **18**, 2804-2816.
15. H. Yu, L. Zhang, S. Jiang, W. Liu, K. Deng, Z. Wang, Y. Xu, H. Wang and L. Wang, *Small*, 2024, **20**, 2406107.
16. X. Gao, Y. Pan, J. Qiu, J. Peng, S. Wang and Y. Zou, *Adv. Funct. Mater.*, 2025, **35**, 2417545.

17. M. Li, T. Wang, W. Zhao, S. Wang and Y. Zou, *Nano-Micro Lett.*, 2022, **14**, 211.
18. L. Zhao, Z. Lv, Y. Shi, S. Zhou, Y. Liu, J. Han, Q. Zhang, J. Lai and L. Wang, *Energy Environ. Sci.*, 2024, **17**, 1291.
19. L. Xiao, W. Dai, S. Mou, X. Wang, Q. Cheng and F. Dong, *Energy Environ. Sci.*, 2023, **16**, 2696-2704.